

# Solitary wave propagation through two-dimensional treelike structures

William J. Falls and Surajit Sen

*Department of Physics, State University of New York, Buffalo, New York 14260-1500, USA*

(Received 24 September 2013; published 27 February 2014)

It is well known that a velocity perturbation can travel through a mass spring chain with strongly nonlinear interactions as a solitary and antisolitary wave pair. In recent years, nonlinear wave propagation in 2D structures have also been explored. Here we first consider the propagation of such a velocity perturbation for cases where the system has a 2D “Y”-shaped structure. Here each of the three pieces that make up the “Y” are made of a small mass spring chain. In addition, we consider a case where multiple “Y”-shaped structures are used to generate a “tree.” We explore the early time dynamical behavior associated with the propagation of a velocity perturbation initiated at the trunk and at the extremities for both cases. We are looking for the energy transmission properties from one branch to another of these “Y”-shaped structures. Our dynamical simulations suggest the following broad observations: (i) for strongly nonlinear interactions, mechanical energy propagation resembles pulse propagation with the energy propagation being dispersive in the linear case; (ii) for strong nonlinear interactions, the tree-like structure acts as an energy gate showing preference for large perturbations in the system while the behavior of the linear case shows no such preference, thereby suggesting that such structures can possibly act as switches that activate at sufficiently high energies. The study aspires to develop insights into the nature of nonlinear wave propagation through a network of linear chains.

DOI: [10.1103/PhysRevE.89.023209](https://doi.org/10.1103/PhysRevE.89.023209)

PACS number(s): 46.40.Cd, 45.70.-n, 43.25.+y, 05.45.Yv

## I. INTRODUCTION

Fermi, Pasta, Ulam, and Tsingou [1,2] studied the evolution of a perturbation in 64 particle mass spring chains where the springs were characterized by harmonic and weakly nonlinear interactions. They showed that when a mode is perturbed, it fails to disperse within the system. Their work suggested that these systems may accommodate nonergodic behavior under certain conditions. This work marked the beginning of studies on the dynamics of nonlinear many-body systems.

Through the past nearly 60 years, a great deal of work has been done on the dynamics of mass spring systems in 1D [3–6] and 2D [7–11], where the masses are connected by springs that typically possess both linear and nonlinear characteristics. Velocity perturbations initiated into these systems often end up as compression (solitary) waves and dilation (antisolitary) waves (see for example in Ref. [12]). Position perturbations can lead to the formation of long-lived localized or weakly localized oscillations or breathers [6,13]. There are scenarios where the solitary and antisolitary waves become breathers [14]. And last but not the least, in the absence of dissipation, these systems eventually end up in the so-called quasiequilibrium state where the system’s dynamics is typically characterized by large energy fluctuations and the absence of equipartitioning of energy [13,15].

In this work we address the dynamics of a Fermi-Pasta-Ulam-like system of masses connected by springs with quadratic and quartic interactions but where the system itself looks like a 2D tree. We ask whether these branched systems are effective energy transmitters and whether the energy can split and recombine as it travels through the branches.

## II. THE MODEL

We first study impulse propagation through our building block, i.e., the “Y”-shaped structure. The layout of our “Y” is given in Fig. 1. There are three chains each made up of  $N_\alpha$

masses connected by springs, and one vertex mass connected to the first mass of each chain by a spring for a total of  $3 \times N_\alpha + 1$  masses, where  $\alpha$  refers to the branch index. The last particle of each chain is connected to an effectively infinite mass that acts as a wall, so we have a total of  $3 \times (N_\alpha + 1)$  springs.

The first chain is kept horizontal while the remaining two chains are arranged to be vertically symmetric at an angle  $\theta$  with respect to the horizon (as seen in Fig. 1). The system is governed by the following Hamiltonian:

$$H = \sum_{\alpha=1}^3 \left( \sum_{i=1}^{N_\alpha} \frac{p_i^2}{2m} + V_{i,i+1} \right) + \frac{p_0^2}{2m} + V_{0,11} + V_{0,21} + V_{0,31}, \quad (1)$$

where the potential between the masses is

$$V_{i,i+1} = \frac{1}{2}k(x_{i+1} - x_i - d_0)^2 + \frac{1}{4}q(x_{i+1} - x_i - d_0)^4, \quad (2)$$

where  $d_0$  is the equilibrium distance between two adjacent particles. The equation of motion for a given particle in one of the three chains is given by

$$m \frac{d^2 x_i}{dt^2} = k(x_{i+1} + x_{i-1} - 2x_i) - q(x_{i+1} - x_i - d_0)^3 - q(x_i - x_{i-1} - d_0)^3, \quad (3)$$

and the equation of motion for the vertex is given by

$$m \frac{d^2 \vec{r}_0}{dt^2} = k[ (|\vec{r}_0 - \vec{r}_{1,1}| - d_0) r_{0\hat{1},1} - (|\vec{r}_0 - \vec{r}_{2,1}| - d_0) r_{0\hat{2},1} - (|\vec{r}_0 - \vec{r}_{3,1}| - d_0) r_{0\hat{3},1} ] + q[ (|\vec{r}_0 - \vec{r}_{1,1}| - d_0)^3 - (|\vec{r}_0 - \vec{r}_{2,1}| - d_0)^3 r_{0\hat{2},1} - (|\vec{r}_0 - \vec{r}_{3,1}| - d_0)^3 r_{0\hat{3},1} ], \quad (4)$$

where  $r_{0\hat{\alpha},1}$  represents the direction vector from the vertex particle to the corresponding particle in branch  $\alpha$ . For particles attached to the vertex mass only the projection of the vertex on the axis of the branch is used. Such a projection eliminates all

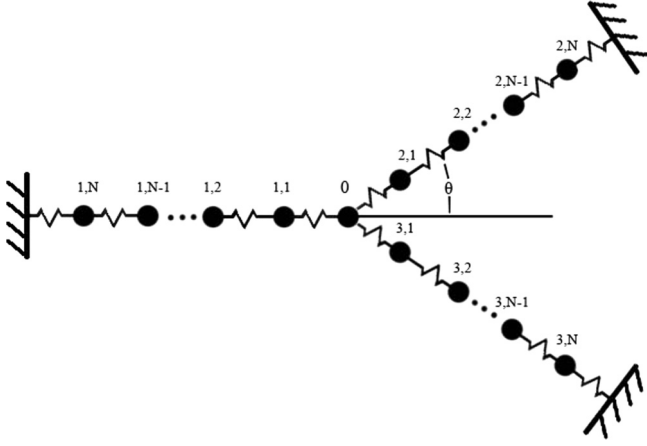


FIG. 1. Physical layout of the “Y”-shaped building block.  $\theta$  is defined from the axis of branch 1 ( $\alpha = 1$ ).

forces perpendicular to the axis of the branch, restraining all the masses in the branches to their original effective axis. The vertex mass, however, is free to move in 2D such that  $r_{0-\hat{\alpha},1}$  varies as the system progresses. The individual strengths of  $q$  and  $k$  will dictate the strength of the nonlinearity and in turn the nonlinearity will dictate the dynamics of the system. For this reason the ratio  $\frac{q}{k}$  will serve as a measure of the overall nonlinearity. A perturbation will be made to the particle in the middle of branch 1 (see Fig. 1), where the initial perturbation is given as

$$E_i = \frac{p_i^2}{2m} + V_{i,i+1}, \quad (5)$$

where  $E_i$  is the total energy of particle  $i$ . The number of particles per chain  $N_\alpha$  is set to 10. Such a size is large enough that compression and dilation pulses can be separated, but it is also small enough that acoustic waves can pass through without dispersing significant amounts of their energy. We envision our physical system as one that may be realized in the laboratory.

To this end we will also assign units to describe the system we construct and to help visualize the dynamics of the system. The equilibrium distance between the particles is set to 1.0 cm and the maximum perturbation velocity used is 1.0 cm/s. The particles that make up the chain will each have a mass of 0.175 g and the maximum energy perturbation used is 8.75 nJ (the maximum energy perturbation is chosen such that the oscillations remain within 3% of the equilibrium length).

Our study focuses on the system’s dynamics in two regimes. The strongly nonlinear coupling limit is chosen such that our maximum initial perturbation strength gives similar orders of magnitude for both the nonlinear and harmonic contribution and the strongly harmonic region is chosen such that the nonlinear contribution will remain at least two orders of magnitude less than that of the harmonic term. The strongly harmonic coupling limit we use in our dynamical studies is  $\frac{q}{k} \leq 1$ , whereas the strongly nonlinear coupling limit we use is  $\frac{q}{k} > 1000$ . While the nonlinear regime may appear extremely large, we should keep in mind that the harmonic coupling still has a significant contribution to the dynamics of the system. In the limit that  $\frac{q}{k} \rightarrow \infty$  the dynamics of the system will be

dictated strictly by the nonlinear coupling, such that the system will initially form only solitary wave (SW) and antisolitary wave (ASW) pairs. This limit is difficult to obtain in the laboratory so we have chosen to omit it from this study.

We initialize the system at zero temperature, so the only energy in the system is that of the perturbation. Once the system has been initialized we model the dynamics by integrating the Newton’s equations of motion using the velocity Verlet predictor corrector algorithm [16]. We use a time step of 100 ns, a smaller time step does not significantly improve the accuracy of the integration. We integrate the system until the initial pulse reaches the far end of the opposite branches and then stop the run. The energy conservation over  $3 \times 10^7$  time steps is to within 0.1 nJ of the initial energy perturbation.

In order to maintain the “Y” branch shape, each individual branch is constrained to move only in the direction of the original alignment of the branch. The vertex mass, as previously stated, is free to move in 2D. Constraining the system as such we lose the dynamics associated with any off-axis forces. The initial pulse is small enough that the off-axis angle will not exceed 3 degrees (as mentioned previously). Therefore, the off-axis dynamics would be several orders of magnitude slower than the pulse dynamics in the branches and would not play any significant role in the time scale of interest here.

For the strongly harmonic coupling case the majority of the energy will move through the system in the form of acoustic waves, although as shown elsewhere [17–20] even in purely harmonically coupled systems nonlinear coupling naturally arises at the vertex, as  $\theta$  itself is dependent on the position of the vertex. For the strongly nonlinear coupling case the majority of the energy at early times will form a compression and dilation pulse traveling in opposite directions. We will start the energy perturbation at particle (1,5) so that the compression pulse travels to the right where it passes into branches 2 and 3 while the dilation pulse travels to the left and reflects off the wall at particle (1,10), where  $(a,b)$  implies particle  $b$  in branch  $a$  (see Figs. 1–3). In order to isolate the compression pulse only the data up to the point when the dilation pulse reaches the vertex will be used. Despite the difference in dynamics between the compression and the dilation pulse, even situations where we reverse the directions of the pulses the resulting energy distribution is the same (see Fig. 6). Therefore, henceforth we will only discuss the compression pulse passing through the vertex for the single-vertex case.

The angle  $\theta$  in the system will be varied between the runs. In order to get a broad understanding of the dynamical behavior of the system we will not just look at the dynamics of the particles but focus on the energy distribution. When the angle is varied symmetrically we only need to look at one branch as the two branches will behave identically. In order to characterize the energy distribution we will define the transmission as the energy that passes from the initially perturbed branch into one of the opposite branches:

$$T = \sum_{i=1}^N \frac{E_i}{E_{\text{tot}}}, \quad (6)$$

where  $\alpha$  equals either 2 or 3. We have defined transmission  $T$  in terms of both potential and kinetic energies in order to avoid

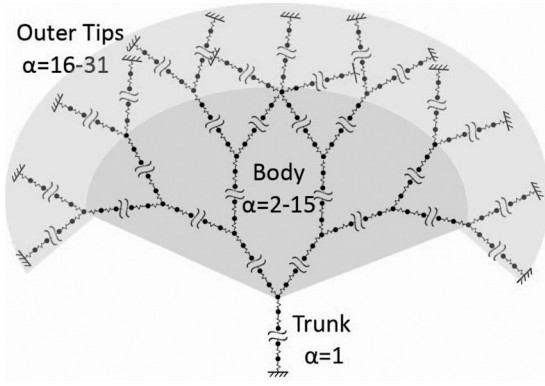


FIG. 2. Physical layout of the larger tree constructed out of “Y”-shaped building block. We have split the system into three regions of interest, the trunk, the body, and the outer tips of the system. For our study we will be concerned with how energy passes from trunk to outer tips and vice versa.

any difficulties with phase effects. Similarly, when the angles are varied independently from each other the transmission will be defined in the same way but will be given for both of the branches.

Having established our building blocks, we can now use them to construct trees. We will do this by attaching a vertex and two more branches to the ends of branches 2 and 3, then we will repeat this process until we have reached the desired size of our system.

It is important to note that branches only interact through vertices in our model. If a tree was constructed that could allow a physical overlap between two branches, there would be no direct interaction between the overlapping branches. This can be seen in the central area of the outer tips in Fig. 2, although there is physical overlap there is no interaction between overlapping branches. The dynamics of the larger system can get considerably more complicated. For this reason, in addition to talking about the transmission of the energy we will also look at the distribution of energy by defining the variances of the calculated average energy per particle from the energy per particle if the energy were perfectly equipartitioned ( $E_{\text{equipartition}}$ ). So we set

$$\sigma = \sum_{i=1}^{\alpha_{\max}} \sum_{i=1}^{N_{\alpha}} \frac{|E_i - E_{\text{equipartition}}|}{(N-1)E_{\text{equipartition}}}, \quad (7)$$

where  $N$  represents the total number of particles in the system,  $\alpha_{\max} \times N_{\alpha} + \frac{\alpha_{\max}-1}{2}$ . We use  $\alpha_{\max} = 31$  in this work, which provides a sufficiently large system to study the dynamics of pulse propagation through such structures and yet is small enough that energy transmission through first passage between the branches can be examined.

While the level of energy distribution is interpreted as variance in a harmonic system, the variance has a different interpretation in a system with nonlinear coupling. Energy can move through a system with nonlinear coupling as a SW or ASW, which under normal circumstances would not split, thus the variance would not change. When a SW or ASW comes in contact with a vertex, some portion of these waves would split (as a function of  $\theta$ ) between the two branches

causing the variance to decrease. As stated previously in the limit that  $\frac{q}{k} \rightarrow \infty$ , our system will produce strictly SW and ASW solutions; therefore, in the strongly nonlinear cases we must consider the possibility of SW solutions existing in the compression pulse and similarly with the ASW and dilation pulse. This means that variance in strongly nonlinear cases can be interpreted as a measure of how many splits the pulse has undergone.

While variance is helpful for getting a broad view of the dynamics of large systems, it is still necessary to understand how the vertices transmit energy when coupled together. In the larger system energy can be localized in three places: the trunk, the body of the system, and the outer tips (see Fig. 2). Since there are different channels for the energy to flow into, we need to define two transmissions rather than one as we did in the case of the single vertex.

$$T_{\text{trunk}} = \sum_{i=1}^{N_{\alpha}} \frac{E_i}{E_{\text{tot}}}, \quad (8)$$

where  $\alpha = 1$  and

$$T_{\text{tips}} = \sum_{\alpha=16}^{31} \sum_{i=1}^{N_{\alpha}} \frac{E_i}{E_{\text{tot}}}. \quad (9)$$

A similar definition can be made for the body of the system; however, here we are concerned with the energy transmission characteristics of the system and thus only the two definitions.

### III. RESULTS OF NUMERICAL EXPERIMENTS

In order to get a complete picture of how our “Y”-shaped building block transmits energy we will do numerical experiments as outlined in Sec. II above. We will probe how an energy perturbation passes through the system as a function of  $\theta$  for strongly harmonic and nonlinear couplings varied symmetrically and asymmetrically. We first probe the system with a single symmetric building block, with  $\theta = 30^\circ$  and  $\frac{q}{k} = 1$  (i.e., strongly harmonic coupling regime). In practice  $\theta = 0$  would relate to a 1D spring mass system with the second half of the chain consisting of particles of twice the mass and springs twice as stiff, so it should be noted that the limiting case is not a uniform one-dimensional chain.

Recall the initial perturbation is made at particle (1,5). For small  $\theta$  we expect the pulse will pass through the vertex into branches 2 and 3 mostly undisturbed. For large  $\theta$  the pulse will have difficulty going through the vertex and hence we expect much of it to reflect back into branch 1. In Fig. 3(a) we see the kinetic energy versus time plotted for particles (1,4), (2,4), and (3,4). The energy moves outwards from the initial perturbation and makes its way through branches 2 and 3. The energy in particles (2,4) and (3,4) are identical, so henceforth we will only concern ourselves with plotting the energy associated with one of the two branches in strongly harmonically coupled systems. It should be noted that we have made many individual runs of these systems to make sure that the results captured are accurate.

Next we study the system again with  $\theta = 30^\circ$  but  $\frac{q}{k} = 1700$  (i.e., in the strongly nonlinear coupling regime), and once again we start the initial perturbation at particle (1,5). In Fig. 3(b) we see the kinetic energy versus time plotted for particles (1,4),

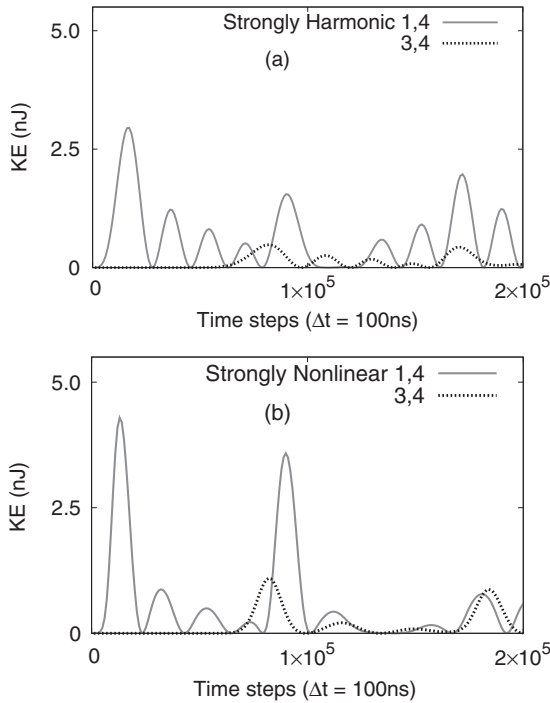


FIG. 3. The dynamics of particles (1,4) and (3,4) (Fig. 1) after particle (1,5) is perturbed are plotted. (a) and (b), respectively, depict strongly harmonic coupling and strongly nonlinear coupling with  $\theta = 30^\circ$ . In both (a) and (b) the energy reaches particle (3,4) with ease, however, in (a) the magnitude of the pulse is significantly smaller than in (b).

(2,4), and (3,4) once again. The results in Fig. 3(b) clearly show that the energy propagates through the branches as an energy bundle. The energy bundle strongly resembles a SW; however, due to our system's small chain size and presence of harmonic coupling the characterization of a SW is extremely difficult. For this reason we will not classify the energy bundle as a SW in this study. Just as before, branches 2 and 3 are identical and hence there is no need to plot the energies in both the branches.

The strongly harmonic coupling between the masses causes acoustic oscillations in the trunk, such oscillations result in the perturbation moving through the chains as an acoustic-like pulse. As we saw above for small  $\theta$ , the vertex did not transmit much of the acoustic-like pulse through the chains. We next repeat the above simulations for a much larger  $\theta$ , such as  $\theta = 80^\circ$ . In Fig. 4(a) we see the strongly harmonic coupling case and in Fig. 4(b) we see the strongly nonlinear coupling case. This time both the strongly harmonic coupling and strongly nonlinear coupling transmit the energy very poorly. The numerical experiments strongly suggest that for large  $\theta$  values, very little energy can get through from the trunk to the tips irrespective of the nature of the interactions between the particles that make up the system. However, over a series of independent runs we find that for smaller  $\theta$  values, nonlinear waves are better suited for efficient energy transport from the trunk to the tips than linear waves. We address this  $\theta$  dependence of  $T$  for both symmetric and asymmetric cases below.

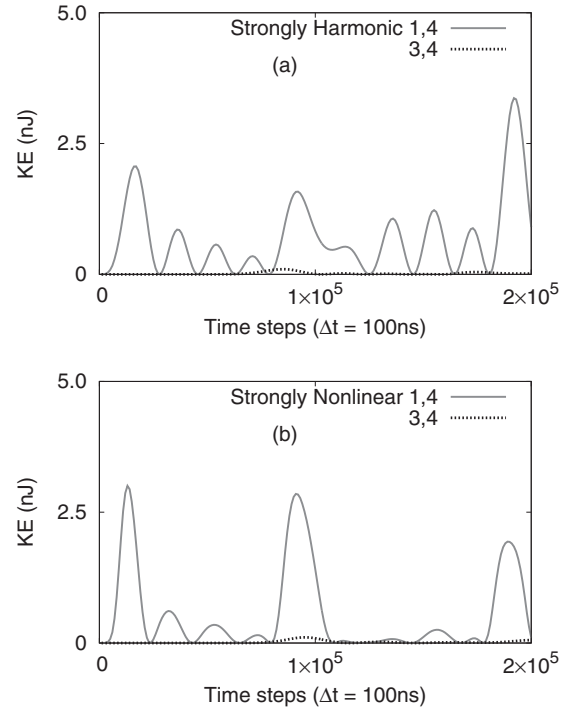


FIG. 4. The dynamics of particles (1,4) and (3,4) (Fig. 1) after particle (1,5) is perturbed are plotted. (a) and (b), respectively, depict strongly harmonic coupling and strongly nonlinear coupling with  $\theta = 80^\circ$ . In both (a) and (b) the energy has difficulty reaching particle (3,4).

To get a complete picture of the transmitted energy's dependence on  $\theta$  we now plot transmission [see Eq. (6)] versus  $\theta$ . Previously we have seen that for a small  $\theta$  the strongly nonlinear coupling transmits energy through the vertex quite well. We also noted that for large  $\theta$  both strongly harmonic and strongly nonlinear coupling transmit poorly. In order to understand the region between the two cases we have seen, we need to see transmission as a function of  $\theta$ . In Fig. 5 we have plotted the transmission as a function of  $\theta$  for both the strongly harmonic case and the strongly nonlinear coupling case. In all of these cases the system is kept vertically symmetric; therefore, only the transmission for a single branch is shown. We see that the shapes of the graphs for the strongly harmonic and strongly nonlinear coupling cases are quite sensitive to the nature of the interactions. Both cases begin to decrease the amount of energy transmitted after the same value of  $\theta = 45^\circ$  or  $\theta = \frac{\pi}{4}$  radians. However, in the strongly nonlinear coupling case we see that the energy passes through small angles much easier than the strongly harmonic case, something we saw first hand in Fig. 3. We have also plotted transmission versus  $\theta$  in Fig. 6 for strongly nonlinear coupling with both compression and dilation pulses. The transmission's dependence on  $\theta$  is identical for compression and dilation; therefore, henceforth we will only show the transmission for compression pulses. It should be noted that there is a small numerical difference in the transmission for compression and dilation; however, we suspect this is an artifact of our system's constraints. Constraining the system to only move in the direction of the original alignment of the branch there is a slight difference in

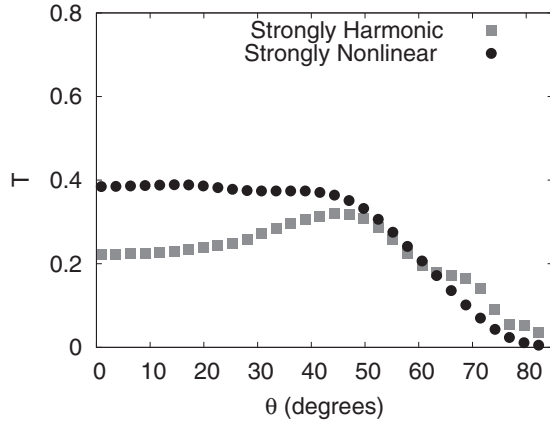


FIG. 5. Transmission [see Eq. (6)] is plotted for both strongly harmonic and strongly nonlinear coupling as  $\theta$  is varied symmetrically. We see that for small  $\theta$  the transmission of energy in the strongly nonlinear case is much higher than the strongly harmonic case. For large  $\theta$  the transmission approaches zero for both strongly harmonic and strongly nonlinear coupling.

the magnitude of the vertex’s projection on the branches for compression and dilation pulses. This difference in the vertex’s projection is most likely the cause of the small numerical difference.

In the strongly harmonic case the transmission increases as  $\theta$  approaches  $45^\circ$ . To better understand this effect we will discuss the large and small limits of  $\theta$ . For small  $\theta$ ,  $r_{0\hat{-}2,1}$  and  $r_{0\hat{-}3,1}$  are almost directly opposed to  $r_{0\hat{-}1,1}$ , making the system stiff in the direction of energy propagation. For large  $\theta$ ,  $r_{0\hat{-}2,1}$  and  $r_{0\hat{-}3,1}$  are almost perpendicular to  $r_{0\hat{-}1,1}$ , so that the projection of the vertex on branches 2 and 3 is small. As the  $\theta$  approaches  $45^\circ$  the system softens allowing larger oscillations of the vertex and more energy to pass through; however, the projection of these oscillations in branches 2 and 3 becomes smaller so eventually the increase tapers off. While this argument should be true for both strongly nonlinear and strongly harmonic cases, the strongly harmonic case is

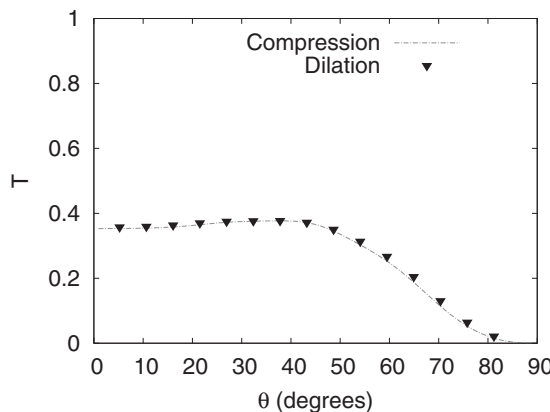


FIG. 6. Transmission [see Eq. (6)] is plotted for strongly nonlinear coupling as  $\theta$  is varied symmetrically for both a compression and a dilation pulse. As we can see the shape of the dependence is identical. It should be noted that there is a slight numerical difference in magnitude.

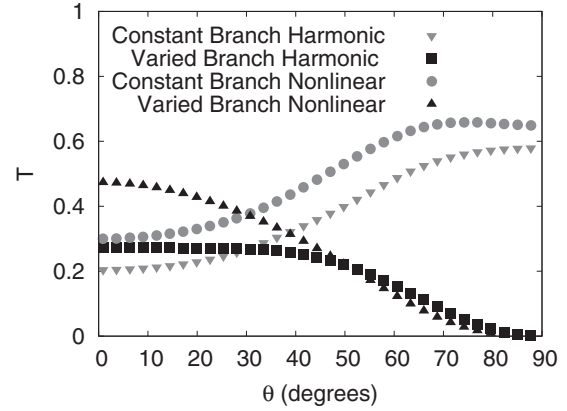


FIG. 7. Transmission [see Eq. (6)] is plotted for both strongly harmonic and strongly nonlinear coupling as  $\theta$  is varied asymmetrically. One branch is varied while the other is kept at a constant  $\theta = 30^\circ$ . In both cases the branch that is closest to the axis of branch 1 ( $\alpha = 1$ ) transmits the most energy.

the only one affected. We can attribute this to the difference between the harmonic and nonlinear potentials. With respect to the harmonic potential the nonlinear potential is weak for small oscillations. In the stiff limit (small  $\theta$ ) strongly nonlinear effects enter when the oscillations are large. As  $\theta$  approaches  $45^\circ$  the system becomes floppier and hence the oscillations become larger; however, since the nonlinear potential increases rapidly the change in the oscillation amplitude is small and the effect of increased energy transmission is hence not seen in the strongly nonlinear case. For large  $\theta$  both cases approach zero transmission, the strongly harmonic coupling case, however, does not approach zero as smoothly as the strongly nonlinear coupling case. In this region, due to the presence of acoustic oscillations in the branches, we expect to see larger oscillations of the vertex mass. The observed behavior is a result of these oscillations.

Next we repeat the above simulations; however, this time the angle is not varied symmetrically, instead the angle for branch 2 will be kept at a constant  $\theta = 30^\circ$  and the angle for branch 3 will be varied from  $0-90^\circ$ . In Fig. 7 we have plotted the transmission as a function of  $\theta$  for both the strongly harmonic case and the strongly nonlinear coupling case. In both strongly harmonic coupling and strongly nonlinear coupling cases the pulse will prefer to transmit to the branch that is closer to the axis of the incoming pulse with more energy being transmitted at small  $\theta$  values when the interactions are strongly nonlinear.

With the behavior of our building block well defined we can now look at larger systems that are made up of these “Y”-shaped structures. Constructing the system as described previously, we will make a system 31 branches large. If the system size is larger, it splits the energy so finely that the branch dynamics begins to approach the timescale of the off-axis dynamics in the single building block case. To simplify the system, all angles in the system were set at  $30^\circ$ .

To explore the short-time dynamics of the overall system we choose to use the variance  $\sigma$  [see Eq. (7)] as a function of time.  $\sigma$  gives us a coarse-grained picture of the dynamics based on the difference between the calculated average energy per particle and the equipartitioned energy per particle obtained

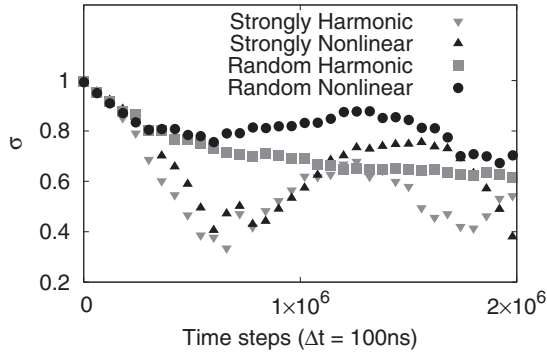


FIG. 8. The variance from equipartition ( $\sigma$ ) is plotted for strongly harmonic and strongly nonlinear coupling, each of these cases are shown with symmetric and random angles separately. For symmetric angles in both cases the variance fluctuates with a frequency characteristic of the size of the system; however, in the strongly harmonic case the magnitude of the oscillation is smaller. Using random angles in the system we see that the strongly nonlinear case still fluctuates its variance; however, in the strongly harmonic coupling case the oscillations are canceled out completely.

using the total energy and  $N$ . In Fig. 8 we have plotted the variance [see Eq. (7)] as a function of time for varying strengths of harmonic and nonlinear couplings.

We can see that for both strongly nonlinear and linear couplings, the system has a tendency to oscillate its variance over the course of the run. A close look at the data shows that the first dip in Fig. 8 coincides with the initial perturbation completing its journey all the way to the tip of the tree structure, i.e., when the initial acoustic pulse has been distributed among all the branches. The strongly harmonic case reveals a second minimum, which coincides with a return of the energy to the tip for a second time. The strongly nonlinear case, however, behaves slightly differently with the value of  $\sigma$  reaching the first minimum at about the same time as that of the harmonic case but then remaining quite significant until somewhat later times (until about  $2 \times 10^6$  time steps). Such behavior arises because unlike in the harmonic case, the smaller the pulse, the slower it moves (as expected for nonlinear waves) and the longer the passage takes and hence the delay in the second minimum in the nonlinear case.

In Fig. 8 we have also plotted the variance as a function of time for varying strengths of harmonic and nonlinear couplings with random asymmetric angles inserted into the building blocks rather than the symmetric angles used previously. The random asymmetric angles vary uniformly from  $\theta = 0-60^\circ$ . Standard Monte Carlo methods were used with a Mersenne twister pseudorandom number generator to create the distribution [21]. The randomness in the angle means that more energy is transmitted in both cases through the branch at the smaller angle with respect to the trunk. In the strongly nonlinear case once a difficult vertex to pass through (both top and bottom  $\theta$  is large) is encountered by the pulse, the pulse simply returns to the initial point of perturbation, which gives rise to the same type of oscillations we saw previously in the variance. In the strongly harmonic case a difficult vertex causes energy to be trapped locally, not only diminishing the oscillations in variance as we saw before but also limiting

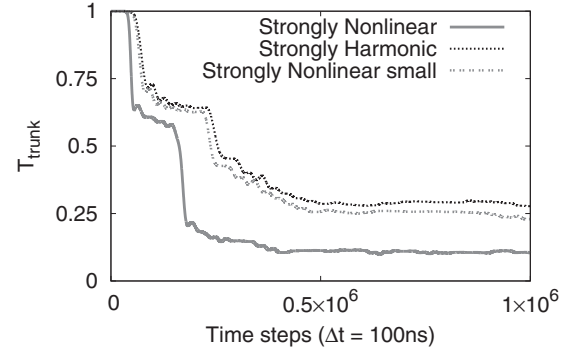


FIG. 9.  $T_{\text{trunk}}$  [see Eq. (8)] is plotted as a function of time for three cases. The maximum perturbation made to the strongly nonlinear system, maximum perturbation made to the strongly harmonic system, and one quarter of the maximum perturbation made to the strongly nonlinear system.

the system from approaching equilibrium. This of course is expected on the basis of results discussed in Figs. 2–4. It is clear that the energy transmission between the branches is such that  $\sigma$  decays quite slowly in time for both cases though it is significantly more slow for the nonlinear case, which means that the system will always have large fluctuations seen in the energy traveling through the various branches.

In Fig. 9 the trunk transmission [Eq. (8)] is plotted for a tree structure as a function of time. Four different cases were run, the maximum perturbation (in order to maintain a small-angle approximation) made on a strongly nonlinear system, the maximum perturbation made on a strongly harmonic system, one-quarter of the maximum perturbation made on a strongly nonlinear system, and one-quarter of the maximum perturbation made on a strongly harmonic system. Both of the strongly harmonic cases gave nearly identical transmission data, so for clarity only one of the strongly harmonic cases is shown in Fig. 9. All of the cases ran show similar dynamics; we can see that in each case there are similar plateaus in the transmission. These correspond to the time it takes for the leading edge of the pulse and then trailing edge to pass through the branch. However, the case of the maximum perturbation made to the strongly nonlinear tree shows a drastic difference in the magnitude of the transmission. In order to track where the energy has gone, though, we need to turn our attention to the outer tips of the system.

In Fig. 10 the tips transmission [Eq. (9)] is plotted for a tree structure as a function of time. The same four cases as above were run, and as before only one strongly harmonic case is shown for clarity. Here we see that once again there is similar dynamics in all of the cases, the same similar plateaus form as first leading edge of the pulse and then later the trailing edge reach the outer tips. Also corresponding with the trunk transmission the case of the maximum perturbation made to a strongly nonlinear system transmits the largest amount of energy into the tips of the system. Clearly there is some dependence on both nonlinearity and perturbation strength for the transmission in the system, so to wrap up our study we will also look at the reverse case.

In Fig. 11 the trunk and tips transmission is plotted for a tree structure as a function of time. Four separate cases were run,

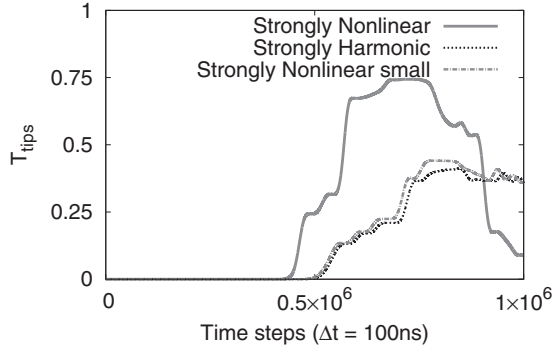


FIG. 10.  $T_{tips}$  [see Eq. (9)] is plotted as a function of time for the same three cases described previously.

the maximum perturbation evenly distributed among the tips of a strongly nonlinear system, the maximum perturbation evenly distributed among the tips of a strongly harmonic system, one-quarter of the maximum perturbation evenly distributed among the tips of a strongly nonlinear system and one-quarter of the maximum perturbation evenly distributed among the tips of a strongly harmonic system. The perturbation strength dependence is not seen in these cases, so only the maximum perturbations were plotted in Fig. 11. In addition to the lack of a dependence on the perturbation strength we also fail to see any dependence on the nonlinearity in the system. Surprising as the results of Fig. 11 are, it should be observed that the original pulse has been split among the tips and hence the pieces are relatively tiny regardless of the strength of the perturbation. Piecing these tiny pieces together to a whole as the energy progresses toward the trunk is not as easily realized as the process of breaking down an incoming pulse from the trunk into the branches.

There are two important results to take away from this. First the broad brush approach of using the variance of the system, a statistical approach, completely misses the important results of the transmission capabilities of the system. Second and most importantly, a strongly nonlinear tree can be used as an effective gate for energy perturbations. A strong pulse made in the trunk can be transmitted strongly to the tips; however, the same pulse made to the tips will not transmit strongly

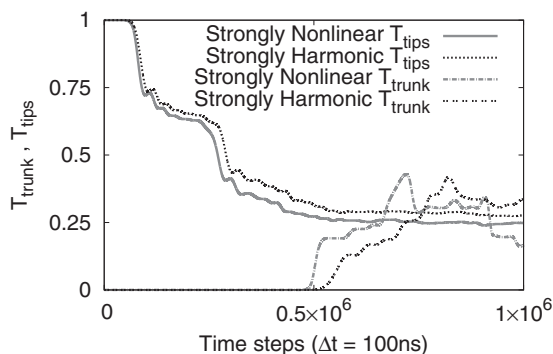


FIG. 11.  $T_{trunk}$  and  $T_{tips}$  are plotted as a function of time. Two cases are shown, the maximum perturbation made evenly distributed among the tips ( $\alpha = 16-31$ ) of a strongly nonlinear system and the tips of a strongly harmonic system.

backwards into the trunk. This allows the system to be used as directional gate for energy. While these results may seem intuitive, the actual results themselves are not immediately obvious from viewing the transmission for a single Y branch.

#### IV. THEORETICAL ARGUMENTS

The oscillatory features in the strongly linear and nonlinear trees shown in Fig. 8 strongly suggest that the larger system recombines energy. In order to understand this, we need to consider how the system progresses through time. Initially, the pulse travels through the system as both an acoustic wave and a nonlinear pulse (as seen previously in Figs. 3 and 4). At each vertex the pulse will split some of their energy between the two branches (the amount of energy split is dependent on  $\theta$  as seen previously). If the branches are symmetric, the energy will be split equally; however, for the case study shown in Fig. 4, the first 0.07 seconds every vertex hit will be symmetric. Once the 0.07 seconds has elapsed, the compression pulse will reach the far end of the system and begin to make its return trip. Each vertex the pulse encounters now is from the opposite perspective. As seen in Fig. 1 this would relate to either a pulse passing from branch 2 into branches 1 and 3 or a pulse passing from branch 3 into branches 1 and 2. Both of these scenarios are that of an asymmetric branch. As we saw in Fig. 7, the pulse will propagate through the branch that has the smallest angle with respect to its current branch, which in this case is the trunk that the pulse initially passed through.

For angles greater than  $\theta = 90^\circ$  a compression of the vertex will result in a dilation of the outgoing branch. This switch between compressing and stretching will cause a compression pulse to become a dilation pulse at the vertex and as stated before both have the same dependence on  $\theta$  for transmission. This scenario applies to both the top and bottom branch, and as long as the system has been kept symmetric, the two pulses pass through the vertex at the same time and recombine some of their energy into one pulse. This process will repeat itself until the pulse makes it back to the initially perturbed branch.

While the tendency to recombine energy is visible in the variance of the system it is also important to note the gating behavior that is visible when plotting transmission in Fig. 9. Without a preference for the direction of transmission the pulse would be able to move back and forth through the system relatively unrestrained (some energy will always be dissipated by harmonic coupling and even in ideal transmission scenarios not all of the energy passes through the vertex) causing the tree structure to be highly ineffective at energy transmission.

If our understanding of how the system behaves is accurate, then we should find that any break in symmetry should decrease the amount of energy recombined. Introducing such a break will result in the pulses being split unevenly between branches, which in turn makes them return to the vertex at slightly different times. When the pulses return they will only be partially recombined. Looking back at the variance of the strongly nonlinear coupling case in the presence of random angles in Fig. 8, the decrease in the second peak corresponds to a decrease in how much energy was recombined. Additionally, when it comes to the variance of the strongly harmonic coupling case in the presence of random angles we see that the peak is completely suppressed. While this simplified

explanation of the process holds true, the behavior is very robust in strongly nonlinear systems.

## V. CONCLUSION

In this study, we set out to discover how a nonlinear pulse behaves on a tree-shaped structure. In order to answer this question, we constructed a two-dimensional tree structure consisting of “Y”-shaped building blocks. These building blocks were made up of masses connected by springs, and arranged in a “Y”-shaped structure with branches joined by a vertex mass. By constraining the individual branches to one dimension, only the vertex was free to move in two dimensions. First, we examined how the building block transmits energy as a function of  $\theta$  in both symmetric and asymmetric cases. Next, we looked at how trees distribute energy perturbations. By performing this analysis, it was found that energy perturbations made in the tree could dissipate and later recombine. In this study we found that the nonlinearity in the system shows a strong preference for passing large energy pulses from its trunk to its tips. This preference limits how much energy will be recombined. Building upon this, we predicted that introducing

symmetry breaking angles into the tree would prevent energy from recombining. To confirm this prediction we examined trees that were constructed using asymmetric building blocks and saw a decrease in the magnitude of the recombined energy.

This study examined a very general problem, but the implications of what we’ve investigated can help in understanding nonlinear wave propagation in an array of more specific problems. First, the tendency to recombine energy perturbations acts as an easy way to characterize the effects of nonlinearity of a system that might otherwise be too complex to classify. The capability of strongly nonlinear tree-like systems to act as ways to distribute energy propagation through multiple channels and to collect energy available via multiple channels suggests the potential for unique ways of directing and capturing energy and may have possible applications. The studies could also be useful when dealing energy propagation through branched structures in the context of biological systems and condensed matter systems.

## ACKNOWLEDGMENT

We acknowledge US Army Research office for partial support of this work through a STIR grant.

- 
- [1] E. Fermi, J. Pasta, and S. Ulam, Los Alamos National Laboratory Report, LA-1940, MAY (1955).
  - [2] E. Fermi, *Phys. Z.* **24**, 64 (1923).
  - [3] J. Zabusky and M. Kruskal, *Phys. Rev. Lett.* **15**, 240 (1965).
  - [4] F. M. Izrailev and B. V. Chirikov, *Statistical Properties of a Nonlinear String* [Institute of Nuclear Physics, Novosibirsk, USSR, 1965 (in Russian)]; *Dokl. Akad. Nauk. SSR* **166**, 57 (1966) [*Sov. Phys. Dokl.* **11**, 30 (1966)].
  - [5] J. Ford, *Phys. Rep.* **213**, 271 (1992).
  - [6] D. K. Campbell, S. Flach, and Y. S. Kivshar, *Phys. Today* **57**, 43 (2004).
  - [7] H. Hirooka and N. Saito, *J. Phys. Soc. Jpn.* **26**, 624 (1969).
  - [8] N. Zabusky, *Comp. Phys. Comm.* **5**, 1 (1973).
  - [9] S. Takeno, *J. Phys. Soc. Jpn.* **59**, 1571 (1990).
  - [10] J. A. D. Wattis, *Phys. Scr.* **50**, 238 (1994).
  - [11] P. G. Kevrekidis, K. Ø. Rasmussen, and A. R. Bishop, *Phys. Rev. E* **61**, 2006 (2000).
  - [12] T. R. Krishna Mohan and S. Sen, *Pramana J. Phys.* **64**, 423 (2005).
  - [13] S. Sen and T. R. Krishna Mohan, *Phys. Rev. E* **79**, 036603 (2009).
  - [14] J. P. Boyd, *Nonlinearity* **3**, 177 (1990).
  - [15] S. Sen, T. R. Krishna Mohan, and J. M. M. Pfannes, *Physica A* **342**, 336 (2004).
  - [16] M. P. Allen and D. J. Tildesley, *Computer Simulation of Liquids* (Clarendon, Oxford, 1987).
  - [17] G. Friesecke and K. Matthies, *Discrete Contin. Dyn. Sys.-Ser. B* **3**, 105 (2003).
  - [18] A. V. Zolotaryuk, P. L. Christiansen, and A. V. Savin, *Phys. Rev. E* **54**, 3881 (1996).
  - [19] B. A. Malomed, P. G. Kevrekidis, D. J. Frantzeskakis, H. E. Nistazakis, and A. N. Yannacopoulos, *Phys. Rev. E* **65**, 056606 (2002).
  - [20] T. Astakhova and G. Vinogradov, *J. Phys. A: Math Gen.* **39**, 3593 (2006).
  - [21] M. Matsumoto and T. Nishimura, *ACM Trans. Model. Comput. Simul.* **8**, 3 (1998).